PNAS RESEARCH ARTICLE | PHYSICS

Optimal transitions between nonequilibrium steady states

Samuel Monter[a], Sarah A. M. Loos[b,c,1], and Clemens Bechinger[a,1]

Affiliations are included on p. 11.

Edited by Christopher Jarzynski, University of Maryland, College Park, MD; received April 29, 2025; accepted August 14, 2025

The optimal control of finite-time processes on the microscale is of significant theoretical and practical interest, particularly for the energy-efficient operation of nanomachines. While previous studies have primarily focused on transitions between equilibrium states, many biologically and technologically relevant processes occur far from equilibrium. In such nonequilibrium settings, memory, a ubiquitous feature in realistic systems, plays an intricate role, as any driving necessarily excites internal memory modes. This motivates a deeper exploration of optimal control strategies in nonequilibrium regimes. Here, we combine experiments, theory, and computational methods to investigate the transition of a colloidal particle confined in an optical trap between two nonequilibrium steady states (NESS). We identify optimal control protocols that minimize the thermodynamic work during the finite-time transition between two NESS. We compare optimal protocols in viscous and viscoelastic fluid environments, which are common in realistic technical and biological processes and introduce memory due to a delayed response. Regardless of the presence of memory effects, optimal protocols consistently balance energy extraction with dissipation minimization. In the presence of memory, optimal control is achieved if the protocol matches the time response of the environment. These findings offer key insights for designing optimal control strategies for finite-time, nonequilibrium processes in complex environments.

optimal control | nonequilibrium steady states | microscopic systems | viscoelastic fluids

Significance

Energetic optimization of finite-time processes is of great theoretical and practical relevance, from small-scale engines and robotics to molecular biology and information processing. To move beyond optimal equilibrium-to-equilibrium transitions, we experimentally and theoretically explore transitions between nonequilibrium steady states that minimize energy expenditure. We address the impact of memory, which plays a particularly intricate role in nonequilibrium settings, as driving inevitably excites memory states. As a model system, we study a colloid driven by optical tweezers through viscous and viscoelastic fluids common in technological and biological contexts. We show that optimal protocols, regardless of fluid type, follow a robust trade-off between energy recovery and dissipation minimization. This insight simplifies the design of energy-efficient control strategies in complex, small-scale systems.

The continued progress for miniaturization has intensified the need of optimal control strategies of devices on the micro- and nanoscale (1–9). Previous theoretical and experimental studies have primarily explored optimal finite-time control protocols for transitions between equilibrium states, revealing unexpected complex and nonmonotonic solutions that often feature discontinuous jumps at the beginning and end of the protocol (8, 10–21). More recently, it has been shown that such solutions are constrained by symmetry principles governing optimal finite-time processes and their associated energy costs (22, 23), although this understanding has so far been limited to equilibrium-state transitions.

In general, nonequilibrium steady states (NESS) are far more prevalent than equilibrium states in both natural and synthetic systems, ranging from biological processes to energy conversion devices (24–26). For molecular and nanoscale machines, efficient transitions between nonequilibrium states are crucial to achieve high performance of their cyclic processes. In the context of nonequilibrium thermodynamics, there is also considerable conceptual interest in the thermodynamics of NESS and the transitions between them (9, 27–32). This motivates our study of finite-time control protocols that drive the transition between two NESS, i.e., $\mathrm{NESS}_i \rightarrow \mathrm{NESS}_f$, with minimum input of work.

In contrast to equilibrium transitions, the maintenance of a NESS requires a constant supply of energy, resulting in significant differences in optimal control strategies. First, the cost functional must extend to infinite times to account for sustained energy input. Second, energetic excitations in the environment prior to the transition process play a crucial role. In particular, for systems with memory, arising from internal degrees of freedom or coupling to a complex fluid environment, a portion of the energy stored in NESS_i can be harnessed to facilitate the transition to NESS_f.

Here, we experimentally and theoretically investigate the finite-time optimal control of a colloidal particle suspended in a liquid and driven by optical tweezers, transitioning between two nonequilibrium states with minimum energy cost. To account for the properties of realistic biological and technical fluids, we consider both viscous (Newtonian) and viscoelastic systems. While simple viscous fluids are characterized by a relaxation dynamics being effectively instantaneous on colloidal timescales, viscoelastic

Author contributions: S.M., S.A.M.L., and C.B. designed research; S.M. and S.A.M.L. performed research; S.M. and S.A.M.L. analyzed data; S.M. designed and conduced the experiment, implemented, performed, and evaluated the numerical optimization and simulations; S.A.M.L. performed the analytical calculations; C.B. designed and supervised the experiment; and S.M., S.A.M.L., and C.B. wrote the paper.

The authors declare no competing interest.

This article is a PNAS Direct Submission.

[1]To whom correspondence may be addressed. Email: sarah.loos@ds.mpg.de or clemens.bechinger@uni-konstanz.de.

Published September 15, 2025.

fluids possess additional slowly decaying internal degrees of freedom due to their mesoscopic structure. As a specific sample of a viscoelastic fluid, we used a worm-like micellar network which has a relaxation time on the order of seconds and which results in a time-delayed response of driven particles, i.e., memory effects. Notably, these slow internal degrees of freedom of the viscoelastic micellar network are not directly controllable (or measurable) in our experiments, meaning they are hidden degrees of freedom.

As a central result of this study, we identify two key principles governing optimal $\mathrm{NESS}_i \to \mathrm{NESS}_f$ protocols: the initial recovery of energy stored in NESS_i and the minimization of dissipation during both the transition protocol and the subsequent steady state. In memory-free systems, this leads to a simple and general optimal protocol consisting of just two instantaneous jumps with no driving in between ("jump–wait–jump"). In systems with memory, however, we find that the switching protocol and the corresponding work depend on the protocol duration—an effect absent in the memory-free case. Since nano- and micro-electromechanical systems (NEMS, MEMS) are frequently operated in complex liquids (biological fluids, polymer solutions, dense colloidal suspensions) with slow relaxation dynamics, we believe our results to be relevant for their energy efficient operation under realistic conditions.

Experimental System

As a testbed for our investigations, we choose a system that is equally accessible in experiment, simulation, and theory. We study a microscopic silica particle of 2.7 μm diameter, suspended in a fluid and confined by a harmonic optical potential $V(X) = \frac{\kappa}{2}(X-\lambda)^2$, where X denotes the particle position and κ the trap stiffness. The (time-dependent) trap center position λ is our control parameter. Experimentally, such potential is realized by an optical trap generated by a laser beam with a wavelength of 532 nm, focused into the sample cell with a 100×, NA = 1.45 objective. Different driving protocols are realized by translating the sample cell along the x-direction relative to the optical trap with a computer-controlled piezo stage according to a time-dependent protocol $\lambda(t)$, with a positional accuracy of 100 nm. Our experiments were carried out in two types of liquids. First, we use a 1:1 mixture of water and glycerol. Due to the effectively instantaneous relaxation of the mixture on colloidal timescales, such a fluid gives rise to a memory-free, i.e., Markovian dynamics of the particle. Second, we use a viscoelastic solution of worm-like micelles with a composition of 5 mM equimolar cetylpyridinium chloride and sodium salicylate in water (33, 34). Such fluids exhibit a structural relaxation time on the order of seconds, giving rise to pronounced memory effects and, consequentially, to non-Markovian particle dynamics (35).

The central problem addressed in this work is the optimal protocol λ^* for transitioning from a constant driving regime with velocity v_i to one with v_f within a finite control period t_s, leading to a transition $\mathrm{NESS}_i \to \mathrm{NESS}_f$. We are interested in the optimal protocol during $0 \le t \le t_s$ that minimizes the average work input. Due to thermal fluctuations, more than 100 measurements are typically recorded to ensure statistically reliable results. For a transition to a final equilibrium state, no work input is required for $t > t_s$ even when the particle has not yet fully relaxed to equilibrium. In contrast, for transitions to a NESS, the relaxation toward the final state continues to contribute to the total work. Formally, this is taken into account by extending the integration limits for the cost functional to infinity (10, 36, 37),

$$W = \left\langle \int_0^\infty \frac{\partial V}{\partial \lambda}\dot{\lambda}\mathrm{d}t \right\rangle, \qquad [1]$$

where $\langle \bullet \rangle$ denotes the noise average.

This integral diverges due to the "housekeeping" work contribution, W_{hk}, required to maintain NESS_f. To avoid the need to deal with an infinite cost functional, we subtract the contribution W_{hk}, and optimize the excess work W_{ex}

$$W_{\mathrm{ex}} = W - W_{\mathrm{hk}} = \left\langle \int_0^\infty \left[\frac{\partial V}{\partial \lambda}\dot{\lambda} - \Theta(t-t_s)P_{\mathrm{hk}} \right] \mathrm{d}t \right\rangle. \qquad [2]$$

Here, $P_{\mathrm{hk}} = \gamma v_f^2$ is the housekeeping power (*Materials and Methods*) , and Θ denotes the Heaviside step function.

Memory-Free Systems

The dynamics of a colloidal particle in a viscous liquid is well described by a memory-free (Markovian) Langevin equation. At small Reynold numbers, the particle comes to an immediate stop (within less than a nanometer) once the applied force is removed, apart from thermal fluctuations. Under such overdamped conditions, the equation of motion for a particle confined in a harmonic potential reads

$$\gamma \dot{X} = -\kappa(X-\lambda) + \xi\,. \qquad [3]$$

Here, γ is the particle friction coefficient, and ξ is a delta-correlated random force with zero mean. Despite the simplicity of Eq. **3**, it has been shown that even for transitions between equilibrium states, the optimal protocol λ^* features discontinuities at $t = 0$ and $t = t_s$ (10). Here, an additional complication arises from the boundary conditions, which constrain only the derivative $\dot{\lambda}$ at $t \notin [0, t_s]$, but give no restrictions on λ at any t.

The key insight for deriving exact solutions is to decompose the problem as follows leveraging its Markovian character. We first calculate the optimal contribution to the excess work from times $t \ge t_s$, $\mathcal{W}^*_{t\ge t_s}$, for an arbitrary system configuration $\lambda(t_s) = \lambda_s$, $x(t_s) = x_s$, where $x = \langle X \rangle$ denotes the noise-averaged particle trajectory. The corresponding solution is derived in *Materials and Methods*. By adding $\mathcal{W}^*_{t\ge t_s}$ to the cost functional, we can reformulate the problem as an optimization problem with open boundaries on the interval $[0, t_s]$, with total cost functional

$$\mathcal{W} = \int_0^{t_s} \frac{\partial V}{\partial \lambda}\mathrm{d}\lambda + \mathcal{W}^*_{t\ge t_s}[x_s, \lambda_s]. \qquad [4]$$

By construction, $\mathcal{W} \le W_{\mathrm{ex}}$, and for the optimal protocol $\mathcal{W}[\lambda^*] = W_{\mathrm{ex}}[\lambda^*]$. Therefore, the optimization can be carried out with respect to $\mathcal{W}$ instead of W_{ex}. As we show in *Materials and Methods* using variational calculus, this optimization problem with open boundaries is solved by the protocol

$$\lambda^*(t) = \begin{cases} v_i t + v_i \tau_\kappa, & t < 0 \\ 0, & 0 \le t \le t_s \\ v_f(t-t_s) - v_f\tau_\kappa, & t > t_s \end{cases}, \qquad [5]$$

where $\tau_\kappa = \gamma/\kappa$ denotes the mean relaxation time of the particle position within the trapping potential. Fig. 1 shows the optimal protocol Eq. **5** and corresponding mean particle trajectory for the special example, $v_i = -v_f$.

Regardless of the values of v_i, v_f, the optimal protocol exhibits a symmetry under a combined transformation of time reversal and exchange of the initial and final state, $v_i \leftrightarrow v_f$. Specifically,

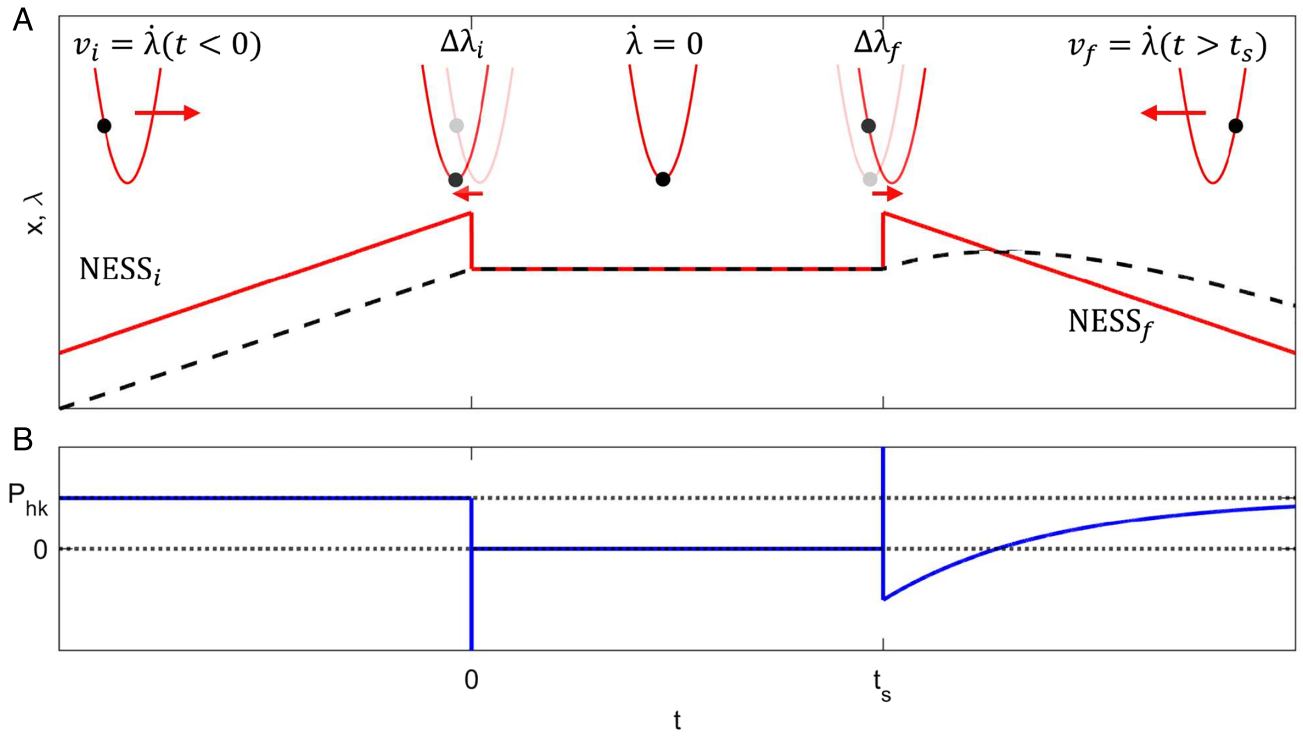

Fig. 1. Optimal protocol for the transition between two NESS. (*A*) Protocol parameter $\lambda^*(t)$ (red solid line) and average particle trajectory $x = \langle X \rangle(t)$ (black dashed line) for the optimal transition NESS$_i$ → NESS$_f$ ($v_i = -v_f$) in a memory-free system. The illustration at the top indicates the motion of the potential and the mean position of the particle at selected times. At $t = 0$ the potential performs a discontinuous jump ($\Delta\lambda_i = -\langle X - \lambda \rangle_{\mathrm{NESS}_i}$) to the particle position, enabling extraction of the potential energy stored in NESS$_i$. During $0 < t < t_s$ the trap remains static. At $t = t_s$, the trap executes another jump opposite to the driving direction of NESS$_f$. The total distance covered by the final jump equals the separation of particle and trap center in NESS$_f$ ($\Delta\lambda_f = -\langle X - \lambda \rangle_{\mathrm{NESS}_f}$). This means that the energy cost for the jump equals the amount of energy that is necessary to reach NESS$_f$. (*B*). corresponding power consumption $P(t)$ for the optimal protocol shown in (*A*). After the initial jump, the system consumes no power. Due to the final jump, the particle's relaxation toward NESS$_f$ is delayed, and during this period P remains below the housekeeping power P_{hk}, resulting in a negative contribution to the excess work. The optimal value of $\Delta\lambda_f$ results from a balance between the cost and benefit of the jump of $\lambda^*(t_s)$. Notably, the jump places the particle at the displacement from the trap center that is exactly opposite from the steady-state displacement. This can be understood by recognizing that $\Delta\lambda_f = -\langle X - \lambda \rangle_{\mathrm{NESS}_f}$ ensures that the invested energy corresponds precisely to what is at the least required to bring the system to NESS$_f$ in any case.

the time-reversed optimal protocol that drives the system from NESS$_i$ to NESS$_f$, denoted $\tilde{\lambda}^*_{i\to f}$, is identical to the time-forward optimal protocol that drives the system from NESS$_f$ to NESS$_i$, denoted $\lambda^*_{f\to i}(t)$. Here, the time-reversal operation is defined as $\tilde{\lambda}(t) := \lambda(t_s - t) - \lambda(0)$, which reverses the time argument and shifts the protocol such that it starts from zero. In this notation, the symmetry can be expressed as $\lambda^*_{i\to f} = \tilde{\lambda}^*_{f\to i}$. The same symmetry is observed for the mean particle trajectories, i.e., $x^*_{i\to f} = \tilde{x}^*_{f\to i}$.

The protocol Eq. **5** involves a jump of the trap of size $\Delta\lambda_i = -v_i\tau_\kappa$ at $t = 0$ followed by a second jump $\Delta\lambda_f = -v_f\tau_\kappa$ at $t = t_s$, with $\dot{\lambda} = 0$ in between. Both jumps are directed opposite to the driving direction of the respective NESS. Remarkably, both jump heights are identical to the distance between the trap and mean particle position in the respective NESS. This implies that the protocol can be fully determined from steady-state measurements alone, without the need to estimate any parameters.

The form of the optimal protocol can be rationalized by examining the corresponding optimal excess work, which is, for arbitrary $v_{i,f}$, given by the following three terms:

$$W^*_{\mathrm{ex}} = -\frac{\kappa}{2}(v_i\tau_\kappa)^2 + \frac{\kappa}{2}(v_f\tau_\kappa)^2 - 2\tau_\kappa\gamma v_f^2. \qquad [6]$$

The first term corresponds to the maximum extractable portion of the potential energy stored in NESS$_i$ (note that, in general, not all of the potential energy can be extracted, as $(\kappa/2)\langle x \rangle^2 \leq (\kappa/2)\langle x^2 \rangle = V$, by the Cauchy–Schwarz inequality). From an energetic point of view, this is ideally achieved by a sudden jump of the optical trap toward the mean particle position. After that, no work on the particle is done until $t = t_s$. Indeed, between the jumps, the particle and trap remain at rest with $\lambda(t) = x(t)$, corresponding to an equilibrium state. The second term in Eq. **6** is the energy expenditure associated with the final jump. The work required to perform the second jump is exactly equal to the potential energy contained in the final steady state, thus representing an unavoidable energy cost that must be supplied to the particle regardless of the protocol. The optimal way is to do it in an instantaneous jump. However, from this perspective, there remain two possible directions of this second jump. By being directed opposite to the motion of NESS$_f$, the jump delays the final relaxation process. This strategy is energetically favorable, since the system reaches its maximum power consumption only after reaching NESS$_f$ (Fig. 1*B*). The last term in Eq. **6** captures the reduction of the excess work arising due to this delayed relaxation. It is equal to twice the relaxation time multiplied by the housekeeping power of NESS$_f$. The height of $\Delta\lambda_f$ results from the trade-off between the energetic cost for the jump and the profit of the subsequent time-delayed convergence to NESS$_f$. Interestingly, neither the shape of the protocol nor the associated

work input depends on the switching interval t_s in memory-free systems.

To experimentally test these analytical predictions, we exploit the fact that the optimal protocol is fully parameterized by the two jump heights $\Delta\lambda_i$ and $\Delta\lambda_f$. Consequently, W_{ex} should exhibit a minimum as a function of these parameters. In our experiments, we chose the initial and final velocities of the NESS to be $v_i = -v_f = 5\ \mu m\ s^{-1}$, with a protocol duration of $t_s = 1$ s, respectively. Fig. 2*A* shows the measured excess work for different pairs of jump heights, represented in a heat map, with a minimum around $\Delta\lambda_i = \Delta\lambda_f = -0.54\ \mu m$. This minimum is in excellent agreement with our analytical result from Eq. **6** (gray lines in Fig. 2*A*). Figure 2*B* displays the measured (symbols) and calculated (solid line) values of W_{ex} for $\Delta\lambda_i = -\Delta\lambda_f$, showing very good agreement. To calculate the theory curve we experimentally measured $\gamma = 0.157\ \mu N\ s\ m^{-1}$ from the relative position of the particle with regard to the trap center in $NESS_i$ and $\kappa = 1.39\ \mu N\ m^{-1}$ was determined from equilibrium measurements of the positional probability distribution. The small systematic shift of the experimental data displayed in Fig. 2*B* toward larger $\Delta\lambda$ can be mainly ascribed to imperfect execution of jumps due to the stage inertia (not from deviations in γ or κ, which we verified by appropriate control simulations). In Fig. 2*C*, we present the protocol and mean particle trajectory for three combinations of jump heights with the blue one being closest to the optimal protocol. Consistent with our discussion of Eq. **5**, we find that the optimal protocol is characterized by the particle remaining nearly stationary between the jumps.

Notably, the optimal control strategy can also be understood from the perspective of minimizing energy dissipation, favoring minimum movement of the particle. Rewriting the total work using the first law of thermodynamics (or, equivalently, by inserting the Langevin equation into Eq. **2**), yields

$$W[x] = Q[x] + \Delta V[x] = \int_0^\infty \gamma \dot{x}^2 \mathrm{d}t + \frac{\gamma}{2}\tau_\kappa(v_f^2 - v_i^2), \quad [7]$$

which reveals that the optimal strategy minimizes particle motion throughout the protocol, consistent with the trajectories shown in Fig. 1. The equivalence of optimizing work and dissipation arises from the fact that we account for the total cost over the entire process until $t \to \infty$.

Systems with Memory

The structural relaxation of viscous liquids is several orders of magnitude faster than the dynamics of a colloidal particle confined in an optical trap. As a result, the relevant slow degrees of motion are entirely governed by the trap motion, i.e., by the control protocol. However, this breaks down when the surrounding liquid has additional degrees of freedom that evolve on comparable or even slower timescales than those of the colloid. Since such degrees of freedom are beyond direct control, the search for optimal protocols becomes considerably more challenging. We expect significant deviations from the memory-free case, as long-lived excitations will influence the thermodynamic cost of driving, which we seek to minimize.

Fluids with slowly decaying internal degrees of freedom are common in natural and synthetic systems. Typical examples include micellar (33, 34, 38) and polymer solutions (39), as well as biological fluids such as blood or mucus (40, 41). In such environments, the motion of a colloidal particle is described by a generalized Langevin (GLE) equation, featuring a memory kernel $\Gamma(t-t')$ replacing the constant friction γ in Eq. **3**

$$\int_{-\infty}^{t} \Gamma(t-t')\dot{X}(t')\mathrm{d}t' = -\kappa(X(t) - \lambda(t)) + \xi(t). \quad [8]$$

As an example of a fluid with time-delayed response, we use a worm-like micellar viscoelastic solution in our experiments (*Materials and Methods*). The choice of such fluid is motivated by its relatively simple relaxation mechanism, compared to, for example, polymer solutions. Over the range of time and length scales relevant to the experiment, the colloidal dynamics is well described by Eq. **3** with a memory kernel consisting of a sum of two exponential decays (38). Using a Markovian Embedding, this GLE can be transformed into an equivalent micro-mechanical model with two hidden (auxiliary) degrees of freedom; see *Materials and Methods* for details. Before conducting experiments in systems with memory, we require a theoretical prediction of the optimal protocol. To develop a versatile approach capable of computing optimal protocols for processes described by GLE Eq. **8** with different memory kernels, we implement a numerical scheme based on automatic differentiation (42). We parameterize the protocol using an artificial neural network (ANN). To numerically obtain optimal protocols, we define a cost function

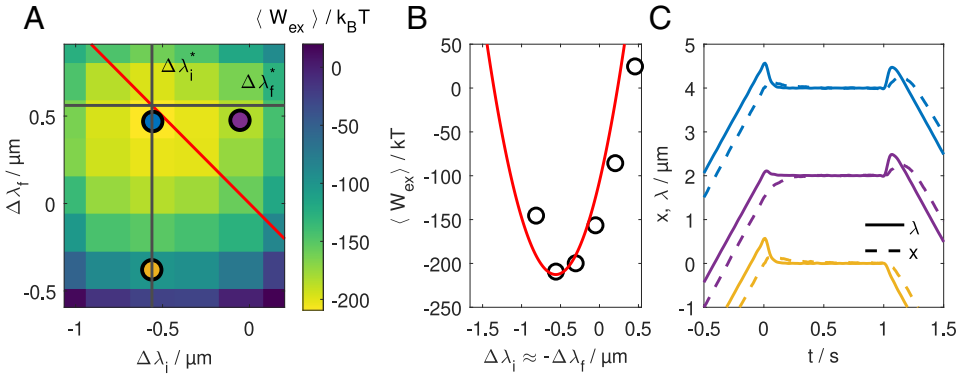

Fig. 2. Experimental validation of theoretically predicted optimal jump heights $\Delta\lambda^*_{i,f} = -\tau_\kappa v_{i,f}$ in viscous system. The average excess work $\langle W_{ex}\rangle$ was measured for various combinations of jump heights $\Delta\lambda_{i,f}$. Here, we fixed initial and final speeds to the same magnitude, for simplicity, $v_i = -v_f = 5\ \mu m^{-1}$. (*A*) Heatmap of $\langle W_{ex}\rangle(\Delta\lambda_i, \Delta\lambda_f)$, showing a pronounced minimum that aligns with the predicted optimum (crossing of black lines). (*B*) Cross-section of $\langle W_{ex}\rangle$ for $\Delta\lambda_i \approx -\Delta\lambda_f$ (open symbols), demonstrating quantitative agreement with theory (red line). The necessary quantities for calculating the theory curve were derived from the experiment which yields $\tau = 0.11$ s. Error bars are smaller than the symbols and thus omitted. (*C*) Example protocols and mean particle trajectories. The blue curves are the case closest to the optimal protocol.

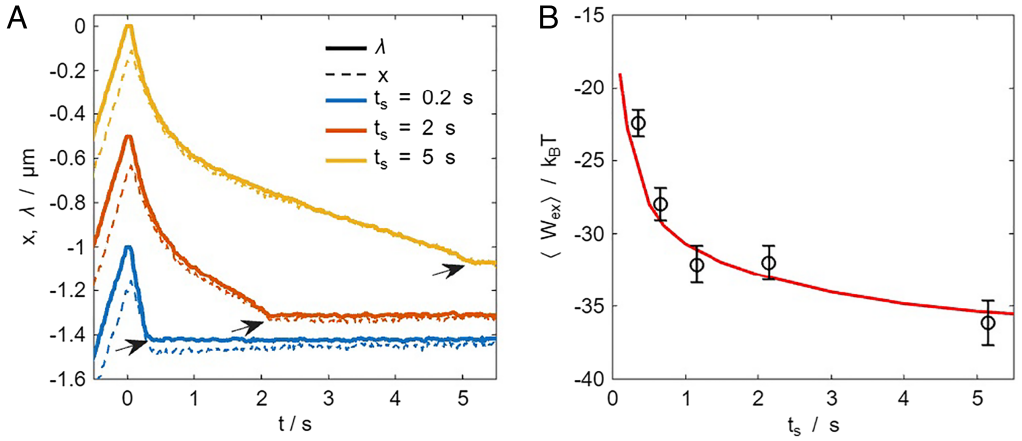

Fig. 3. Optimal protocols in a viscoelastic fluid. (*A*) Three representative optimal protocols λ^* (full lines) for NESS-to-equilibrium switching ($v_i = 1$ μm s^{-1}, $v_f = 0$). Protocols are optimized via automated differentiation using material parameters extracted from calibration measurements. The corresponding mean particle trajectories are shown as dashed lines. Only in case of the shortest switching interval $t_s = 0.5$ s a continued particle motion beyond the control period, suggesting that the residual energy stored within the slow degrees decreases with increasing t_s. (*B*) Measured mean excess work as function of the switching interval t_s (black symbols. Error bars represent $\sqrt{\langle(W_{ex} - \langle W_{ex}\rangle)^2\rangle/N_{meas}}$). Simulation results of $\langle W_{ex}\rangle$ (red line), computed with the material parameters extracted at the end of the measurement series are in good agreement with the experimental data. For longer control periods, the excess work decreases, as more energy can be extracted from slow degrees of freedom that are or only indirectly accessible.

that takes the state of the ANN as input and yields W_{ex} as output. The calculation of the cost function requires three steps: first, generation of a protocol from the ANN, second a Brownian dynamics (BD) simulation probing the resulting motion of the driven particle in the viscoelastic fluid, and finally, computation of the work by integrating Eq. **2**. We optimize the protocol by minimizing the cost function using a gradient descent algorithm, with gradients computed using automatic differentiation, following the strategy presented in ref. 13. The material-specific parameters required for the BD simulation are extracted from fits to calibration measurements. For more detailed descriptions regarding the fitting and optimization procedure, see *Materials and Methods*. There, we also present a comparison between exact solutions and numerical predictions for a simplified dynamics with just one hidden degree of freedom, showing excellent agreement. The exact solutions are obtained using the same strategy as for the viscous case described above. From these extracted model parameters, the relevant relaxation times of the viscoelastic fluid are determined to be $\tau_1 = 0.6$ s and $\tau_2 = 7.7$ s.

We start our investigations by considering the transition between a NESS$_i$ with $v_i = 1$ μm^{-1} to an equilibrium state, i.e., $v_f = 0$. This choice facilitates comparison with experiments by avoiding large spatial displacements of the colloidal particle that are otherwise required to reach a NESS. Unlike in viscous liquids, where optimal protocols are independent of the control period t_s, memory effects introduce a clear dependence on t_s. This is illustrated in Fig. 3*A*, which shows how the optimal protocol λ^* varies with t_s. The protocols have a very distinct form to the memory-free case, and in particular, no longer exhibit the zero-driving regime between the jumps (where $\lambda = \langle X\rangle$), but instead are characterized by a nonzero $\dot{\lambda}$ throughout.

Experimentally realizing the optimal protocols yields the corresponding mean particle trajectories $x(t)$, shown as dashed lines in Fig. 3*A*. Remarkably, the particle's mean position slightly leads the optical trap during the transition (see arrows in Fig. 3*A*). Such behavior, which is never observed in memory-free systems (Fig. 2), indicates that the elastic energy stored in the viscoelastic fluid during NESS$_i$ is partially transferred back to the particle and extracted as work during the protocol. With increasing t, such energy transfer to the particle decreases which explains the decreasing difference between $x(t)$ and $\lambda^*(t)$. In contrast to the viscous case, the particle motion slightly continues even after the protocol is completed (see, e.g., blue curve in Fig. 3*B*). This is also a result of the slowly relaxing fluid which affects the particle motion even beyond t_s.

Fig. 3*B* shows the experimentally obtained values of $\langle W_{ex}\rangle$, which are in good agreement with simulation results, within the experimental errors. The primary source of experimental error arises from the inertia of the piezo table, which causes small deviations from the predicted discontinuity in the protocol at $t = 0$. To account for slow variations (about 15%) in the material parameters over the course of the approximately 48 h lasting measurement period, the experimental routine loops six times over the shown values of t_s, recording 20 trajectories per iteration to ensure sufficient statistics. The red line represents the simulated values of $\langle W_{ex}\rangle$ using the material parameters extracted at the end of the total measurement series. Notably, the predicted decrease of $\langle W_{ex}\rangle$ as a function of t_s is well captured. For the longest tested protocol duration, $t_s = 5$ s, which approaches the slowest timescale of the system, $\langle W_{ex}\rangle$ appears to saturate.

To gain a better understanding of optimal transitions in systems with memory, we numerically investigated the following transition scenarios: acceleration ($v_{i,f} > 0, v_i < v_f$), deceleration ($v_{i,f} > 0, v_i > v_f$), an example of which is shown in Fig. 3, and reversal ($v_i > 0, v_f = -v_i$). For each case, we generated the optimal switching protocols by our AD approach, and computed the corresponding excess work over a wide range of protocol durations $t_s \in [0.01, 100]$ s, exceeding the relevant intrinsic relaxation time scales of our system. The results are summarized in Fig. 4. The qualitative t_s-dependent behavior of λ^* and W_{ex}, as observed experimentally, is preserved across all simulated cases. As expected, when t_s exceeds the longest memory time of the system, λ^* converges toward the protocol of a viscous (memory-free) system. In all cases, $\langle W_{ex}\rangle$ saturates at short and long t_s and varies on a timescale roughly set by the relaxation times of the viscoelastic fluid. The saturation value for $t_s \to 0$ (horizontal line) is derived in *Materials and Methods*; see Eq. **50**.

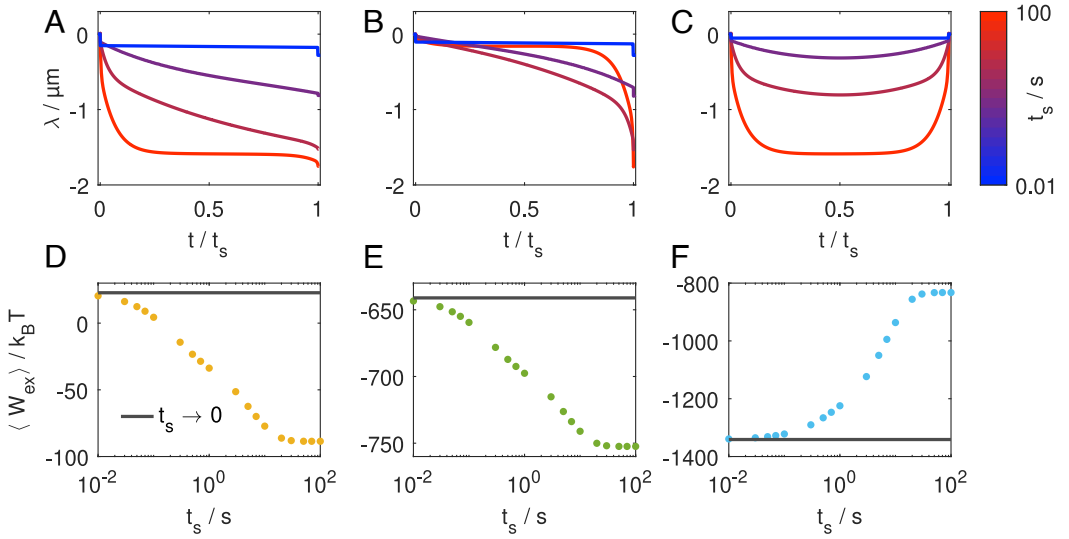

Fig. 4. Optimal protocols and excess work for transitions between different NESS (NESS$_i$ → NESS$_f$), obtained using neural networks and automatic differentiation. Top row, (*A*–*C*) Predicted optimal protocols $\lambda^*(t)$ for a range of t_s. Bottom row, (*D* and *E*) corresponding excess work $\langle W_{ex}\rangle(t_s)$. Each column represents a different transition scenario: Left column (*A* and *D*): deceleration, $v_i = 1$ μm s^{-1}, $v_f = 0.1$ μm s^{-1}; middle column (*B* and *E*): acceleration, $v_i = 0.1$ μm s^{-1}, $v_f = 1$ μm s^{-1}, right column (*C* and *F*): reversal, $v_i = 1$ μm s^{-1}, $v_f = -1$ μm s^{-1}. For acceleration and deceleration $\langle W_{ex}\rangle$ decreases with increasing t_s (*D* and *E*), while the protocols cover a larger distance, indicating a stronger interaction with the slow degrees of freedom. For reversal, $\langle W_{ex}\rangle$ follows the opposite trend (*F*). For all cases, $\langle W_{ex}\rangle$ converges to analytical limit for $t_s \to 0$ (black lines).

Interestingly, in all cases except the reversal ($v_f = -v_i$), longer switching intervals lead to a reduction of $\langle W_{ex}\rangle$, whereas the reversal scenario shows the opposite trend. This implies that, when the switching interval is not fixed, different limits yield optimal solutions depending on the transition scenario.

Longer switching durations allow for a more extended (implicit) interaction between the controlled and uncontrolled degrees of freedom. For the case of a deceleration ($v_i > v_f$), this enables the recovery of a larger fraction of the elastic energy stored in the uncontrolled modes before it is dissipated. Similarly, during a prolonged acceleration ($v_i < v_f$), the slow degrees of freedom can be displaced further from their final configuration in NESS$_f$, thereby reducing the work through extended relaxation. In contrast, for the reversal case ($v_f = -v_i$), the elastic deformation (i.e., excitation) stored in NESS$_i$ pulls the particle toward the driving direction of NESS$_f$. Over a prolonged switching duration, this elastic energy dissipates as heat, making it increasingly costly to force the transition.

The general principle discussed in Eq. 7 for the memory-free case—that optimal protocols are those that minimize particle motion—also extends to systems with memory. Specifically, rewriting the work functional using the first law of thermodynamics yields

$$W[x] = Q[x] + \Delta V[x] = \int_0^\infty \gamma \dot{x}^2 \mathrm{d}t + \int_0^\infty \int_{-\infty}^t \Gamma(t-t')\dot{x}(t')\dot{x}(t)\mathrm{d}t'\mathrm{d}t + \Delta V, \quad [9]$$

which clearly indicates that minimizing particle motion leads to minimum work by minimizing dissipation, as in the viscous case. The second term accounts for dissipation due to memory effects, and its structure confirms that any motion, past or present, adds to the energetic cost.

Strikingly, as in the memory-free case, we also find that the optimal protocol from NESS$_i$ to NESS$_f$, denoted $\lambda^*_{i\to f}$, is identical to the time-reversed optimal protocol from NESS$_f$ to NESS$_i$, denoted $\tilde{\lambda}^*_{f\to i}$. Likewise, the corresponding mean trajectories satisfy $x^*_{f\to i} = \tilde{x}^*_{f\to i}$. Importantly, this symmetry, which holds for all tested cases, is only observed for the optimal protocols. It reflects a deeper reversibility structure in the space of optimal driving protocols between NESS. The symmetry property is consistent with and can be seen as a weaker form or generalization of the time-reversal symmetry $\lambda^* = \tilde{\lambda}^*$ reported in ref. 22, where $v_i = v_f = 0$.

In addition, the corresponding work of the forward and backward protocol W and $\tilde{W}$ are identical up to a constant. As an immediate consequence (for a derivation, see *Materials and Methods* Eqs. **52**–**60**) the sum of excess work of the forward and backward process is given by

$$W_{ex} + \tilde{W}_{ex} = W(t > t_s) + \tilde{W}(t > t_s). \quad [10]$$

This suggests that the excess work contributions up to t_s exactly cancel when reversing the direction of the protocol. This symmetry property seems to be a general feature of optimal solutions.

Discussion

Using experiments, theory, and numerical tools, we investigated finite-time optimal switching protocols inducing the transition between two NESS (NESS$_i$-to-NESS$_f$), that minimize the associated work expenditure. The experiments were performed with a colloidal particle suspended in a fluid and confined to a driven optical trap. To study the influence of slow, hidden degrees of freedom (memory) that are not directly controllable during the experiment, we compared optimal protocols in viscous and viscoelastic fluids. In general, the optimal protocols exhibit jumps at the beginning and the end. Independent of the presence of memory effects, our findings indicate that the specific form of optimal protocols arises from a balance between energy extraction and dissipation minimization. In particular, the delayed relaxation to NESS$_f$ proves energetically beneficial, as

the power consumption reaches its maximum in the steady state. The possibility of extracting energy from the hidden degrees of freedom in a system with memory causes the optimal protocol and work to depend on the duration of the protocol only under such conditions.

Beyond the boundary conditions considered here, which only constrain the driving speed, alternative types of boundary conditions for the protocol could be of interest. For example, one could consider optimal problems that enforce full convergence of the particle to the final NESS within a fixed time window, similar to previous studies for equilibrium states (43). In systems with memory, such conditions are expected to lead to more intricate optimal strategies. Finally, the quest for optimal protocols can also be extended to more complex systems. With state-of-the art numerical methods, like the automatic differentiation tool (13) used here, one can explore optimal driving in nonlinear rheological fluids with a velocity-dependent friction coefficient, or in systems with complex particle interactions. Our approach combining experiments, computational tools, and theory provides a foundation for such future studies of soft and active matter systems far from equilibrium.

Materials and Methods

Experimental Methods.

Optical trap setup. The optical tweezers setup utilizes a 532 nm laser (Coherent Verdi V2). With a $\lambda/2$-plate and a polarizing beam splitter the laser power is adjusted to 250 mW at the entrance aperture of the acousto-optic deflector (AOD, AA opto-electronics DTSXY-400). The AOD is used to modulate the intensity of the laser, i.e., the trap stiffness, for individual measurements. After blocking the zeroth diffraction order, the laser intensity behind the AOD dropped below 100 mW. An Olympus Apochromat MPLAPON-Oil $100\times$ NA $= 1.45$ objective was utilized to focus the laser beam into the sample cell. A three-axis piezo-driven stage (piezoconcept LT3) was used to horizontally translate the sample. A voltage signal with a 10 kHz sampling rate from a PCIe card (National Instruments PCIe-6351) controlled the stage position through the analog input, achieving a lateral resolution of 100 nm. The resulting position of the stage was recorded using its analog output signal. A small lateral offset between the set and the actual measured positions is observed for fast positional changes $\gtrapprox 10\ \mu\mathrm{m s}^{-1}$. In all experiments, the temperature of the sample was kept constant at 25.2 ± 0.1 °C. This is achieved by performing experiments in a laboratory with air conditioning (± 0.5 °C). To further suppress temperature fluctuations and drifts, the sample holder and objective are kept in a temperature window of ± 0.1 °C using feedback controlled resistive heaters (Okolab). A digital camera (Basler ace 2 a2A3840-45umPRO) recorded images through the objective that is also used for tweezing. For image acquisition, a frame rate of 100 frames per second was chosen.

Sample preparation. To prepare the viscoelastic solution equimolar amounts of cetylpyridinium chloride monohydrate (CPyCl) and sodium salicylate (NaSal) were dissolved in millipore water. The solution was kept stirring on a hotplate at 40 °C to allow the micellar network to equilibrate. In this study, we used an 6 mM solution.

2.73 μm diameter SiO_2 spheres (microParticles GmbH) were dispersed in either a water-glycerol mixture (volumetric ratio 1:1) or in the before-mentioned viscoelastic solution using an ultrasonic bath to prepare samples for experiments. Glass capillaries with an inner diameter of 100 μm (CM Scientific) were then filled with the dispersion using capillary forces. The prepared samples are sealed with wax and epoxy resin. Before performing measurement, the samples were kept in the measurement setup for more than two hours to allow full thermalization.

Measurement Procedures. Our experiments were obtained by the following measuring procedure: a single micro-particle is first captured in the optical trap. The trap is then translated relative to the fluid according to the chosen protocol. The optical trap stiffness was kept constant in our measurements and determined to 1.4 and 4.5 $\mu\mathrm{N\ m}^{-1}$ for measurements in viscous and viscoelastic fluids respectively. The relative translation of the optical tweezers is achieved by translation of the sample with a piezo-stage and keeping the laser focus position fixed. Although this yields smaller maximal translation velocities compared to a steering of the optical trap via, e.g., an AOD, our approach has several advantages: the optical path of the trap remains unchanged during translation, preventing any spatial changes to its shape and stiffness. Furthermore, since the optical trap is stationary in the camera's reference frame, we can use a high-resolution objective with only a rather small field of view.

Protocols were repeated in forward and backward direction which avoids the need of large translational displacements when repeating measurements. To ensure complete relaxation, an equilibration period of $t_{rel} = 3$ s for the viscous fluid and $t_{rel} = 40$ s for the viscoelastic fluid was included before each protocol of duration t_s. Also, the trap velocity of NESS_i is maintained over t_{rel} seconds to guarantee that the system has reached the steady state. This leads to following single steps of stage velocity:

$$v_{stage} = \begin{cases} 0 & \text{for } t \le t_{rel} \\ -v_i & \text{for } t_{rel} < t \le 2\,t_{rel} \\ -\dot{\lambda}(t) & \text{for } 2\,t_{rel} < t \le 2\,t_{rel} + t_s \\ -v_f & \text{for } 2\,t_{rel} + t_s < t \le 3\,t_{rel} + t_s \\ v_i & \text{for } 3\,t_{rel} + t_s < t \le 4\,t_{rel} + t_s \\ \dot{\lambda}(t) & \text{for } 4\,t_{rel} + t_s < t \le 4\,t_{rel} + 2\,t_s \\ v_f & 4\,t_{rel} + 2\,t_s < t \le 5\,t_{rel} + 2\,t_s \end{cases} \quad [11]$$

In order to compute meaningful averages, protocols were repeated 300 times in the viscous fluid and 120 times in the viscoelastic fluid. During a parameter scan, the process is repeated multiple times to account for any drifts. More specifically for the measurements in the viscoelastic fluid we loop six times over the whole range of t_s. Measurements for each t_s are repeated 20 times during an individual loop.

Evaluation of experimental data. The particle position is tracked by analyzing video recordings captured at a frame rate of 100 fps using a custom tracking algorithm based on ref. 44. The position of the piezo-stage and the exposure active signal of the camera are recorded at 10 kHz using a PCIe card. This allows to synchronize the stage and particle positions a posteriori. The work done during a single protocol is calculated using the Stratonovich formalism (Eq. **1**). Since the trajectory is only sampled at finite intervals $\Delta t = 0.01$ s, the integral transforms into a sum:

$$W = \sum_{i=1}^{N-1} \frac{\frac{\partial V}{\partial \lambda}\big|_{t_{i+1}} + \frac{\partial V}{\partial \lambda}\big|_{t_i}}{2} \Big[\lambda(t_{i+1}) - \lambda(t_i)\Big]. \quad [12]$$

The work was computed for individual trajectories and then averaged.

In the case of $v_f \neq 0$ it is necessary to subtract the housekeeping work W_{hk} from this expression in order to calculate the excess work W_{ex}. In our experiments, this is only necessary for the experiments in the viscous fluid. Here, $W_{\mathrm{hk}} = \gamma v_f^2 t_{rel}$. The friction coefficient γ is determined from the relative position of the particle to the trap center in NESS_i and the trap stiffness according to $\gamma = \frac{\kappa}{v_i}\langle x - \lambda\rangle_{\mathrm{NESS}_i} = 0.157\ \mu\mathrm{N\ s\ m}^{-1}$. It was calculated for different v_i and subsequently averaged.

A summary of all important measurement and model parameters is given in Table 1.

Optimal Protocol in Viscoelastic Fluid.

Microscopic Maxwell model. The memory properties of the viscoelastic solution used in our experiments are well described by a GLE (Eq. **8**). Another way of describing the memory properties of the complex fluid is by introducing fictitious hidden degrees of freedom that are coupled to the observed particle. In our previous study (22) one hidden degree of freedom was sufficient to match the experiments, because the overall particle displacements were small, i.e., on the order of the particle's diameter. In our present study, the particle is dragged off tens of diameters to reach the steady state. Thereby, additional elastic modes

Table 1. Overview of measurement and model parameters

Parameters	v_i	v_f	t_{rel}
$\kappa = 1.39\ \mu N\ m^{-1}$ $\gamma = 0.16\ \mu N\ s\ m^{-1}$	$5\ \mu m^{-1}$	$-5\ \mu m^{-1}$	3 s
$\kappa = 4.48\ \mu N\ m^{-1}$ $\gamma_t = 0.23, 0.18, 0.19\ \mu N\ s\ m^{-1}$ $\kappa_{b1} = 0.90, 0.69, 0.57\ \mu N\ m^{-1}$ $\gamma_{b1} = 0.55, 0.41, 0.32\ \mu N\ s\ m^{-1}$ $\kappa_{b2} = 0.04, 0.03, 0.03\ \mu N\ m^{-1}$ $\gamma_{b2} = 0.28, 0.21, 0.17\ \mu N\ s\ m^{-1}$	$1\ \mu m\ s^{-1}$	0	40 s

The parameters for the viscous case in the top part of the table are extracted directly from the experiment from the NESS position. The parameters of the Maxwell model are extracted by the fitting routine described in *Fitting of Model Parameters*. The three values given for each parameter correspond to different points in time during the experiment, reflecting the aging effects of the viscoelastic medium. The first values is extracted prior to the measurement run to determine the parameters for the optimization, the second and third extracted from the first and last measurement used for Fig. 3.

are excited. From a previous work (38) on the used viscoelastic fluid, it is known that this makes it necessary to use two hidden degrees of freedom in order to capture the system dynamics. This leads to the three coupled overdamped Langevin equations, which have the general structure of a microscopic Maxwell model

$$\gamma_t \dot{X} = -\kappa(X - \lambda) - \kappa_{b1}(X - X_{b1}) - \kappa_{b2}(X - X_{b2}) + \xi_t \quad [13]$$

$$\gamma_{b1}\dot{X}_{b1} = -\kappa_{b1}(X_{b1} - X) + \xi_{b1} \quad [14]$$

$$\gamma_{b2}\dot{X}_{b2} = -\kappa_{b2}(X_{b2} - X) + \xi_{b2}\,. \quad [15]$$

Here, $X_{b1/b2}$ denote the positions of the two fictitious "bath particles" that model slowly relaxing (hidden) degrees of freedom in the viscoelastic environment. The fictitious particles are coupled to the real one by a linear spring with constant $\kappa_{b1/2}$ and have a friction coefficient $\gamma_{b1/b2}$.

Fitting of model parameters. To predict optimal control protocols for experiments, we first extract the parameters of the Maxwell model (γ_t, γ_{b1}, κ_{b1}, γ_{b2} and κ_{b2}) from experiments. Specifically, we either conduct calibration measurements with the same sample before a parameter scan or use actual data from the parameter scan, to fit simulation to measurements. The calibration experiment is designed to resemble the driving that will be performed in the actual experiment of the optimal control process later on. It consists of an initial equilibration period of 40 s followed by driving with constant velocity $v_i = 1\ \mu m^{-1}$ for 40 s. Subsequently, a jump over $-0.5\ \mu m$ is performed. Thereafter, the particle is allowed to relax for another 40 s while the trap stands still. The experiment is repeated 20 times and the resulting particle trajectories are averaged $\langle X(t)\rangle = x_{exp}(t)$. The stiffness of the trap $\kappa = 4.47\ \mu N\ m^{-1}$ is extracted from the equilibration period. Then a simulation of Eqs. **13**–**15** with a set of starting parameters is performed using the recorded protocol $\lambda_{exp}(t)$. Since we are only interested in the average particle trajectory, the simulation is performed without noise. The result is the simulated particle trajectory x_{sim}. The mismatch of simulation and experiment is quantified by the sum over the absolute difference of the measured and simulated particle trajectory:

$$C = \sum_{t=t_{start}}^{t_{end}} |x_{sim}(t) - x_{exp}(t)|. \quad [16]$$

We use this as a cost function for a gradient descent optimization of the model parameters. The gradient for the optimization is provided by calculating the derivative of C with respect to the model parameters using JAX (42). The optimized parameters are listed in Table 1. A comparison between the measured mean particle trajectories and simulations is shown in Fig. 5. As can be seen from Fig. 5*D*, the biggest source of deviation is the softening of the jump due to the inertia of the stage.

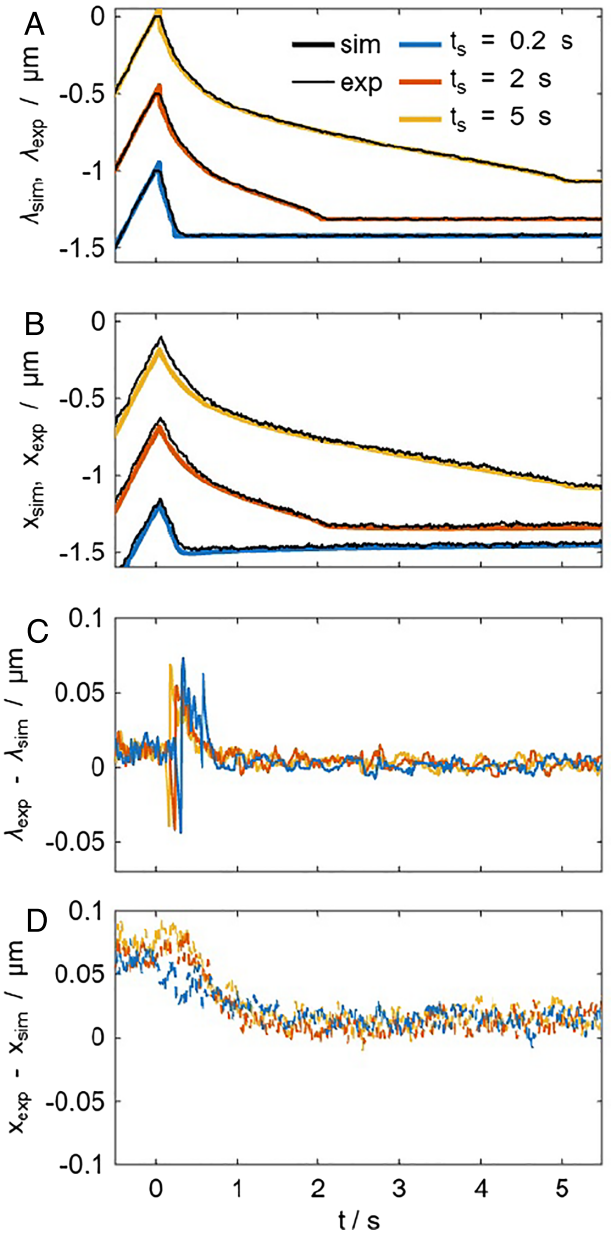

Fig. 5. Comparison of protocols (*A*) and average particle trajectories (*B*) from experiments and simulations in the viscoelastic fluid and simulations. The simulations use parameters fitted to the calibration measurements which were run prior to the execution of optimal protocols (see Table 1 first parameter set for viscoelastic fluid). Sharp features of the stage signal are smoothed out in experiments due to the inertia of the stage. The main features of the average particle trajectories are well captured by the simulation. (*C* and *D*) show the differences between simulation and experiment for protocol and trajectory respectively. For the protocols (*C*), the biggest difference arises due to the before mentioned imperfect jump around $t \approx 0$. When comparing particle positions (*D*) the deviations for $t < 0$ arise due to aging effects between parameter extraction and protocol execution (to get an impression of the aging effects during the experiment, see Table 1 for the viscoelastic fluid). The simulations are run with the parameter set also used for the protocol prediction.

To validate our fitting routine we have compared it to a trust-constr method from the python package scipy.minimize using squared errors and found very good agreement (not more than $\pm 2\ \%$).

Numerical prediction of optimal protocols via Automatic Differentiation. To predict the optimal protocol for the viscoelastic solution described by Eqs. **13**–**15**, we perform numerical optimization using automatic differentiation

To parameterize the protocol $\lambda(t)$ we use an ANN. The ANN has a single input (t/t_s) and output node (λ) and has one fully connected hidden layer with 8 nodes. We use a tanh activation function to increase the nonlinear character of the ANN. From analytic derivations (Eqs. **39** and **41**) we know that at the end of the protocol $\langle X-\lambda\rangle_{t=t_s} = -\langle X-\lambda\rangle_{\mathrm{NESS}_f}$, i.e. the average distance between particle position and trap center must be equal to the negative distance of particle and trap center in NESS_f. With this constraint, we can realize jumps at $t=t_s$ by resetting the trap to the required position. Jumps at $t=0$ emerge more easily by fixing the final state of NESS_i to $\lambda(t=0)=0$. A nonzero output of the ANN for $t=0$ then leads to a discontinuity in $\lambda(t)$. To numerically obtain optimal protocols, we define a cost function that takes the state of the ANN as an input and yields W_{ex} as output. The calculation of the cost function requires three steps: first, the protocol is determined by evaluating the ANN in its current state; second, a BD simulation is run with this protocol. To save computation time the particle positions X, X_{b1}, and X_{b2} are initialized in the NESS_i according to

$$\langle X-\lambda\rangle_{\mathrm{NESS}_i} = -\frac{\gamma_t+\gamma_{b1}+\gamma_{b2}}{\kappa}v_i \qquad [17]$$

$$\langle X_{b1}-X\rangle_{\mathrm{NESS}_i} = -\frac{\gamma_{b1}}{\kappa_{b1}}v_i \qquad [18]$$

$$\langle X_{b2}-X\rangle_{\mathrm{NESS}_i} = -\frac{\gamma_{b2}}{\kappa_{b2}}v_i. \qquad [19]$$

Simulations are performed without noise as we are only interested in average quantities and the system is linear. Finally, the excess work is calculated in three parts. For the initial jump and the continuous protocol ($0 \le t < t_s$) Eq. **2** is integrated numerically using the Stratonovich convention. The final jump $\Delta\lambda_f$ is calculated from the difference in potential energy

$$\mathrm{d}V = V(x(t_s),\lambda(t_s)+\Delta\lambda_f) - V(x(t_s),\lambda(t_s)) \qquad [20]$$

The excess work during relaxation to NESS_f for $t > t_s$ is calculated from the analytical expression given in Eq. **48**. This is a big advantage since the simulation can be terminated just after the protocol ends. A full simulation of the relaxation is computationally expensive due to the long relaxation times of the system.

Using the python library JAX (42), we can derive this complex function with respect to the current state of the ANN. The obtained gradient can then be used to perform a gradient descent optimization of the ANN in order to reach the optimal parameterization which gives the optimal protocol. For optimization, we use the implementation of the ADAM optimizer in the Optax package (45). The parameters of the optimizers were set to $\beta_1 = 0.95$ and $\beta_2 = 0.99$, all other parameters were left at the default setting. The learning schedule is adapted for different ranges of t_s in order to aid quick convergence.

To validate the numerical routine we compare the predicted optimal protocol to exact results for a system with a single hidden degree of freedom (Fig. 6). The exact results are obtained using the same optimization strategy as described in the next section for the viscous case: decomposing the optimization problem into contributions before and after t_s, and solving the open boundary optimization problem on $t \in [0, t_s]$ via Euler–Lagrange equations. To apply this procedure to the viscoelastic case, we work with the Markovian representation of the dynamics given in Eqs. **13** and **14** with $\kappa_{b2} = 0$. As shown in Fig. 6, the numerical results are in excellent agreement with our exact solution. As the analytical approach rapidly grows in complexity with additional degrees of freedom, we employ the flexible numerical scheme for systems with two or more bath variables.

The code used for the numerical predictions is available in a compact version here (46).

Exact Solution for Viscous Case.

Mean trajectory and power in NESS. The general solution of the Langevin equation Eq. **3** for the mean trajectory, denoted by $x = \langle X\rangle$, for an arbitrary protocol λ, is given by

$$x(t) = x_0 e^{-t/\tau_\kappa} + \tau_\kappa^{-1}\int_0^t e^{-(t-t')/\tau_\kappa}\lambda(t')\mathrm{d}t', \qquad [21]$$

where x_0 denotes the mean particle position at the initial time $t=0$. For linear driving $\lambda = vt$, this leads to the expression

$$x(t) = x_0 e^{-t/\tau_\kappa} + v[t-\tau_\kappa(1-e^{-t/\tau_\kappa})] \qquad [22]$$

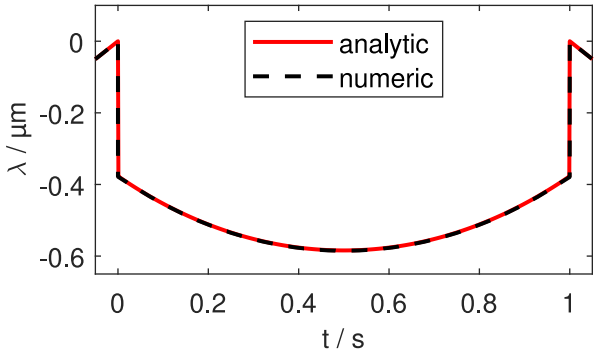

Fig. 6. Comparison between the exact solution and numerical results obtained using our approach that combines ANN with automatic differentiation, for optimal protocol in a system with one hidden degree of freedom Eqs. **13** and **14** with $\kappa_{b2} = 0$). The example shown here corresponds to a transition from $v_i = 1\ \mu\mathrm{m}^{-1}$ to $v_f = -1\ \mu\mathrm{m}^{-1}$, with $\kappa = 1\ \mu\mathrm{N\,m}^{-1}$, $\gamma_t = 0.246\ \mu\mathrm{N\,s\,m}^{-1}$, $\gamma_{b1} = 0.49\ \mu\mathrm{N\ s\ m}^{-1}$, $\kappa_{b1} = 0.42\ \mu\mathrm{N\ m}^{-1}$. Both results agree very well, validating our numerical method.

with $\tau_\kappa = \gamma/\kappa$. After an initial relaxation period, the mean position approaches its steady state value

$$x(t) = v(t-\tau_\kappa) \qquad [23]$$

so that in a NESS

$$x-\lambda = \langle X-\lambda\rangle = -v\tau_\kappa\,. \qquad [24]$$

Accordingly, the power in a NESS with $\dot\lambda = v$ is simply

$$\dot W = P_{\mathrm{hk}} = \frac{1}{t_2-t_1}\kappa\int_{t_1}^{t_2}\dot\lambda(\lambda-x)\mathrm{d}t = \gamma v^2\,. \qquad [25]$$

Excess power after quench to linear driving, from arbitrary initial condition. We consider a linear driving process $\lambda = \lambda_s^+ + v_f\hat t$ with $\hat t = t - t_s$, with some arbitrary initial conditions $x(\hat t=0) = x_s$. According to Eq. **22**, the mean particle trajectory is given by

$$x(\hat t) = (x_s-\lambda_s^+)e^{-\hat t/\tau_\kappa} + v_f[\hat t - \tau_\kappa(1-e^{-\hat t/\tau_\kappa})] + \lambda_s^+\,. \qquad [26]$$

Correspondingly, the excess work during the linear driving process ($t > t_s$) is given by

$$\begin{aligned}\mathcal{W}_{t>t_s} &= \int_0^\infty\left[\dot W - P_{\mathrm{hk}}\right]d\hat t\\ &= \int_0^\infty\left[\kappa\dot\lambda[\lambda(\hat t)-x(\hat t)] - \gamma v_f^2\right]d\hat t\\ &= \int_0^\infty\left\{-\kappa v_f(x_s-\lambda_s^+ + v_f\tau_\kappa)e^{-\hat t/\tau_\kappa}\right\}d\hat t\\ &= -\gamma v_f(x_s-\lambda_s^+ + v_f\tau_\kappa)\,. \end{aligned} \qquad [27]$$

To allow for the possibility of a discontinuity in λ, i.e., a jump of the trap from λ_s^- to λ_s^+, at the onset of this linear driving process at time $t=t_s$, we add the work input associated with this possible jump, leading to the total excess work of

$$\mathcal{W}_{t\ge t_s} = -\gamma v_f(x_s-\lambda_s^+ + v_f\tau_\kappa) + \frac{\kappa}{2}(\lambda_s^+ - x_0)^2 - \frac{\kappa}{2}(\lambda_s^- - x_0)^2\,. \qquad [28]$$

Now, optimizing the last expression with respect to λ_s^+, we find that the minimum excess power is

$$\mathcal{W}^*_{t\ge t_s} = \frac{\kappa}{2}(\tau_\kappa v_f)^2 - \frac{\kappa}{2}(\lambda_s^- - x_0)^2 - 2\gamma v_f^2\tau_\kappa\,, \qquad [29]$$

which is achieved if the trap exhibits a jump of optimal height $\Delta\lambda = \lambda_0^+ - \lambda_0^- = -\tau_\kappa v_f + x_s - \lambda_0^-$ at $t = t_s$.

Optimal protocol via Euler–Lagrange. To find the minimum work protocol, we optimize $\widetilde{\mathcal{W}}$, defined in Eq. **4**, using variational calculus. Consistent with the main text, we set the origin of the coordinate axis to the trap center just after $t = 0$, so that,

$$\lambda_0^+ = 0,\ x_0 = x(0) = -\Delta\lambda_0 - v_i\tau_\kappa\,, \tag{30}$$

where x_0 follows from Eq. **23**, with a potential jump of the trap of height $\Delta\lambda_0 = \lambda_0^+ - \lambda_0^-$ at $t = 0$. Using a Lagrange multiplier to constrain the solution to the manifold of the system's dynamics, the cost functional Eq. **4** gives rise to the Lagrangian:

$$\mathcal{L} = \kappa\dot{\lambda}^*(\lambda^* - x) + \Lambda(t)[\gamma\dot{x} + \kappa x - \kappa\lambda]\,. \tag{31}$$

For this Lagrangian, the Euler–Lagrange equations yield

$$\frac{\partial\mathcal{L}}{\partial x} - \frac{\mathrm{d}}{\mathrm{d}t}\frac{\partial\mathcal{L}}{\partial\dot{x}} = -\kappa\dot{\lambda} + \kappa\Lambda - \gamma\dot{\Lambda} = 0 \tag{32}$$

$$\frac{\partial\mathcal{L}}{\partial\lambda} - \frac{\mathrm{d}}{\mathrm{d}t}\frac{\partial\mathcal{L}}{\partial\dot{\lambda}} = -\kappa\Lambda + \kappa\dot{x} = 0 \tag{33}$$

$$\frac{\partial\mathcal{L}}{\partial\Lambda} - \frac{\mathrm{d}}{\mathrm{d}t}\frac{\partial\mathcal{L}}{\partial\dot{\Lambda}} = -\kappa\lambda + \kappa x + \gamma\dot{x} = 0\,. \tag{34}$$

This set of linear differential equations admits the solution

$$\Lambda^* = c \tag{35}$$

$$x^*(t) = ct + x_0 \tag{36}$$

$$\lambda^*(t) = ct + \frac{\gamma}{\kappa}c + x_0, \tag{37}$$

for $t \in [0, t_\mathrm{s}]$, with some unknown constant c. Note that except for the special case $c = -\frac{\kappa}{\gamma}x_0$, these solutions feature a jump of the trap at time $t = 0$. Finally, we determine c by minimizing the total excess work $\mathcal{W}$ (Eq. **4**) for the solution Eq. **35**, with respect to c. The first contribution to $\mathcal{W}$ stems from times until t_s. This is obtained by computing the integral in Eq. **4** for the optimal solution Eq. **35**, taking into account the work expenditure of the initial jump at time $t = 0$, which is $\Delta V_0 = \frac{\kappa}{2}(\tau_\kappa c)^2 - \frac{\kappa}{2}(v_i\tau_\kappa)^2$, which depends on c. Notably, through $x^*(t)$ and $\lambda^*(t)$, the constant c also parameterizes the contribution to the excess work from times $t \geq t_\mathrm{s}$, $\mathcal{W}^*_{t\geq t_\mathrm{s}}$, given in Eq. **29**.

Taken together, this yields the optimal value of the cost functional Eq. **4**

$$\mathcal{W}^* = \gamma t_\mathrm{s}c^2 + \frac{\kappa}{2}(\tau_\kappa c)^2 - \frac{\kappa}{2}(\tau_\kappa c)^2 + \mathcal{C}, \tag{38}$$

where we have encapsulated in the summand $\mathcal{C}$ all terms that are independent of c (and are thus irrelevant for the last step of the optimization). $\mathcal{W}^*$ has a unique minimum at $c = 0$. Plugging this into Eq. **35** reveals a striking feature: The solution between $t = 0$ and $t = t_\mathrm{s}$ is independent of the parameters $v_1, v_2, \kappa, \gamma, t_\mathrm{s}$, and given by a *jump–wait–jump* solution:

$$\lambda^*(t) = \begin{cases} v_i t + v_i\tau_\kappa, & t < 0 \\ 0, & 0 \leq t \leq t_\mathrm{s} \\ -v_f\tau_\kappa + v_f(t - t_\mathrm{s}), & t > t_\mathrm{s} \end{cases}, \tag{39}$$

characterized by two jumps at $t = 0$ and $t = t_\mathrm{s}$:

$$\Delta\lambda_0^* = -v_i\tau_\kappa,\ \dot{\lambda}(0 < t < t_\mathrm{s}) = 0,\ \Delta\lambda_{t_\mathrm{s}}^* = -v_f\tau_\kappa\,. \tag{40}$$

Notably, $|\Delta\lambda_0^*|$ and $|\Delta\lambda_{t_\mathrm{s}}^*|$ correspond exactly to the mean displacement of the particle from the trap center in the respective NESS; see Eq. **24**. The corresponding mean particle trajectory reads

$$x^*(t) = \begin{cases} v_i t, & t < 0 \\ 0, & 0 \leq t \leq t_\mathrm{s} \\ v_f[(t - t_\mathrm{s}) - 2\tau_\kappa(1 - e^{-(t-t_\mathrm{s})/\tau_\kappa})] & t > t_\mathrm{s}, \end{cases}\ . \tag{41}$$

The optimal excess work expenditure is

$$\mathcal{W}^* = \frac{\kappa}{2}(v_f\tau_\kappa)^2 - \frac{\kappa}{2}(v_i\tau_\kappa)^2 - 2\tau_\kappa\gamma v_f^2 = W_\mathrm{ex}^*\,. \tag{42}$$

As discussed in the main text, this expression shows that the optimal excess work is given by the difference in potential energy of the two NESS, minus the energy savings during the relaxation process ($t > t_\mathrm{s}$). The specific expression of the latter can be rationalized as follows. γv_f^2 is the NESS power, while $2\tau_\kappa$ is a proxy for the relaxation period during which the particle is effectively slowed down by the protocol (it roughly takes τ_κ to relax from 0 to the steady state displacement $-v_f\tau_\kappa$, and another τ_κ to relax from the initial displacement $v_f\tau_\kappa$ to 0).

Exact Solutions for Viscoelastic Case.

Quench to constant driving regime from arbitrary initial condition, case with memory. We model the dynamics by the 2-bath-variable (Maxwell) model given in Eqs. **13**–**15**, here written as

$$\dot{x} = -a(x - \lambda) - \sum_i a_i(x - x_{bi}) \tag{43}$$

$$\dot{x}_{bi} = -b_i(x_{bi} - x). \tag{44}$$

with $i \in \{1, 2\}$, $a = \kappa/\gamma, a_i = \kappa_{bi}/\gamma, b_i = \kappa_{bi}/\gamma_i$, and $\lambda = vt$. To find analytical solutions, we first transfer to a comoving frame of reference by introducing the variables $y = x - vt + (v/a)\,(1 + \sum_j a_j/b_j)$ and $y_i = x_{bi} - vt + v/b_i + (v/a)\,(1 + \sum_j a_j/b_j)$, where the dynamics can be written in Matrix form as

$$\dot{\boldsymbol{Y}} = \mathbb{A}\boldsymbol{Y}, \quad \text{with} \tag{45}$$

$$\boldsymbol{Y} = \begin{pmatrix} y \\ y_1 \\ y_2 \end{pmatrix},\ \mathbb{A} = \begin{pmatrix} -(a + a_1 + a_2) & a_1 & a_2 \\ b_1 & -b_1 & 0 \\ b_2 & 0 & -b_2 \end{pmatrix}. \tag{46}$$

In this frame of reference, the dynamics is identical to a system of harmonically coupled particles y, y_1, y_2, confined by a trap acting on y. Such system asymptotically equilibrates to $\boldsymbol{Y}(t) \to 0$, corresponding to the NESS solutions

$$x = vt - \frac{v}{a}\Big[1 + \sum_j \frac{a_j}{b_j}\Big],\ x_{b,i} = vt - \frac{v}{b_i} - \frac{v}{a}\Big[1 + \sum_j \frac{a_j}{b_j}\Big]. \tag{47}$$

Before reaching the NESS, the general solution of Eq. **45** for arbitrary $t > 0$ is $\boldsymbol{Y} = \boldsymbol{Y}(0)e^{\mathbb{A}t}$, for any given initial conditions $\boldsymbol{Y}(0) = (y_0, y_{10}, y_{20})^T$. We transform this solution $\boldsymbol{Y}$ back to the lab frame, and plug it into the cost functional Eq. **2**. Performing the integral, we compute the excess work during the relaxation to the NESS, and find

$$\begin{aligned} W_\mathrm{ex}^{t>t_\mathrm{s}} = -\frac{v}{k\kappa_{b1}\kappa_{b2}}\big\{&\gamma_2^2\kappa_1(\kappa + \kappa_{b2})v \\ &+ \kappa_{b2}\big[\gamma_1^2(\kappa + \kappa_{b1})v + \gamma\kappa_{b1}(\gamma v + \kappa x_0) + \gamma_1\kappa_{b1}(2\gamma v + kx_{b1,0})\big] \\ &+ \gamma_2\kappa_{b1}\kappa_{b2}\left(2(\gamma + \gamma_1)v + \kappa x_{b2,0}\right)\big\}. \end{aligned} \tag{48}$$

Here, $x_0, x_{b1,0}$ and $x_{b2,0}$ are the initial conditions for the three degrees of freedom in the lab frame, with the origin at the trap center at the beginning of the relaxation process.

Excess work for $t_\mathrm{s} \to 0$. If $t_\mathrm{s} \to 0$, the protocol can only execute one instantaneous jump. The overall excess work is composed by the cost of the jump plus the contribution from the subsequent relaxation to the new NESS. For the latter, we can use Eq. **48** with $v \to v_f$. The initial conditions $\{x_0, x_{bi,0}\}$ in Eq. **48** can be replaced by the relative position in the initial NESS minus the jump distance, i.e., $x_0 = x^{\mathrm{NESS,i}} - \Delta\lambda$, respectively; which is given in Eq. **47** with $v \to v_i$. The total amount of work is this adjusted equation for $W_\mathrm{ex}(t > t_\mathrm{s})$ plus the change in potential energy through the jump:

$$\Delta V = \frac{\kappa}{2}(x^{\mathrm{NESS,i}} - \Delta\lambda)^2 - \frac{\kappa}{2}(x^{\mathrm{NESS,i}})^2. \tag{49}$$

Taken together, for $t_\mathrm{s} \to 0$, the excess work approaches

$$W_{\mathrm{ex}} = \Delta\lambda \frac{\gamma\,\gamma_1\,\gamma_2[\kappa_{b1}\,\kappa_{b2}/(\gamma\gamma_1) + (\kappa_{b1}/\gamma + \kappa_{b1}/\gamma_1)(\kappa_{b2}/\gamma_2)]v_f}{\kappa_{b1}\kappa_{b2}} + \Delta V. \quad [50]$$

The optimal jump height $\Delta\lambda^*$ is then found from the extrema of $W = W_{\mathrm{ex}}^{t>t_s} + \Delta V$ with respect to $\Delta\lambda$, leading to the optimal jump height of

$$\Delta\lambda^* = -\frac{(\gamma + \gamma_1 + \gamma_2)}{k}(v_f + v_i), \quad [51]$$

with the total instantaneous friction, $\gamma_{tot} = \gamma + \gamma_1 + \gamma_2$. Hence, in the limit $t_s \to 0$, the optimal protocol is identical to the memory-free case (with the corresponding instantaneous total friction γ).

Symmetry of Work. Here, we derive Eq. **10**. The constant connecting forward and backward excess work can be deducted by splitting W_{ex}:

$$W_{\mathrm{ex}}(t_s) = \tilde{W}_{\mathrm{ex}}(t_s) + C \quad [52]$$

$$W(0 \le t \le t_s) + W(t > t_s) = \tilde{W}(0 \le t \le t_s) + \tilde{W}(t > t_s) + C. \quad [53]$$

Using the relation between forward and backward work during the protocol an expression for C follows.

$$W(0 \le t \le t_s) = -\tilde{W}(0 \le t \le t_s) \quad [54]$$

$$2W(0 \le t \le t_s) + W(t > t_s) - \tilde{W}(t > t_s) = C. \quad [55]$$

From this we can further follow:

$$W_{\mathrm{ex}} + \tilde{W}_{\mathrm{ex}} = W_{\mathrm{ex}} + \tilde{\tilde{W}}_{\mathrm{ex}} + \tilde{C} \quad [56]$$

$$= W_{\mathrm{ex}} + W_{\mathrm{ex}} + 2\tilde{W}(0 \le t \le t_s) + \tilde{W}(t > t_s) - \tilde{\tilde{W}}(t > t_s) \quad [57]$$

$$= 2W_{\mathrm{ex}} - 2W(0 \le t \le t_s) + \tilde{W}(t > t_s) - W(t > t_s) \quad [58]$$

$$= 2W(t > t_s) + \tilde{W}(t > t_s) - W(t > t_s) \quad [59]$$

$$W_{\mathrm{ex}} + \tilde{W}_{\mathrm{ex}} = W(t > t_s) + \tilde{W}(t > t_s). \quad [60]$$

Data, Materials, and Software Availability. Simulation code has been deposited in Github (47) and Zenodo (46). Raw data can be obtained from Zenodo (48).

ACKNOWLEDGMENTS. S.A.M.L. acknowledges funding by UK Research and Innovation under the UK government's Horizon Europe funding Guarantee (Grant No. EP/X031926/1), and by the Corpus Christi College, Cambridge through a research fellowship (Non-Stipendary Research Fellowship). This research was further supported in part by Grant NSF PHY-2309135 to the Kavli Institute for Theoretical Physics. C.B. acknowledges funding by the European Research Council through the Advanced Grant BRONEB (No. 101141477).

Author affiliations: [a]Department of Physics, University of Konstanz, Konstanz 78457, Germany; [b]Department of Applied Mathematics and Theoretical Physics, University of Cambridge, Cambridge CB30WA, United Kingdom; and [c]Max Planck Institute for Dynamics and Self-Organization, Göttingen 37077, Germany

1. B. Wang, Y. Zhang, L. Zhang, Recent progress on micro- and nano-robots: Towards in vivo tracking and localization. *Quant. Imaging Med. Surg.* **8**, 461–479 (2018).
2. D. Lucente, A. Manacorda, A. Plati, A. Sarracino, M. Baldovin, Optimal control of an electromechanical energy harvester. *Entropy* **27**, 268 (2025), extraced power from noise (macro) with electronic circuit.
3. S. Tafoya, S. J. Large, S. Liu, C. Bustamante, D. A. Sivak, Using a system's equilibrium behavior to reduce its energy dissipation in nonequilibrium processes. *Proc. Natl. Acad. Sci. U.S.A.* **116**, 5920–5924 (2019), optimal protocol for hairpin folding, generalized friction approach.
4. D. Gupta, S. H. Klapp, D. A. Sivak, Efficient control protocols for an active Ornstein–Uhlenbeck particle. *Phys. Rev. E* **108**, 024117 (2023).
5. L. Cocconi, B. Mahault, L. Piro, Dissipation-accuracy tradeoffs in autonomous control of smart active matter. *New J. Phys.* **27**, 013002 (2025).
6. M. H. H. Pontius *et al.*, Magnetically powered microwheel thrombolysis of occlusive thrombi in zebrafish. *Proc. Natl. Acad. Sci. U.S.A.* **121**, e2315083121 (2024).
7. J. Bechhoefer, Feedback for physicists: A tutorial essay on control. *Rev. Mod. Phys.* **77**, 783–836 (2005).
8. J. Alvarado, E. Teich, D. Sivak, J. Bechhoefer, Optimal control in soft and active matter. arXiv [Preprint] (2025). https://arxiv.org/abs/2504.08676 (Accessed 2 July 2025).
9. D. Guéry-Odelin, C. Jarzynski, C. A. Plata, A. Prados, E. Trizac, Driving rapidly while remaining in control: Classical shortcuts from Hamiltonian to stochastic dynamics. *Rep. Prog. Phys.* **86**, 035902 (2023).
10. T. Schmiedl, U. Seifert, Optimal finite-time processes in stochastic thermodynamics. *Phys. Rev. Lett.* **98**, 108301 (2007).
11. S. Blaber, M. D. Louwerse, D. A. Sivak, Steps minimize dissipation in rapidly driven stochastic systems. *Phys. Rev. E* **104**, L022101 (2021).
12. S. Blaber, D. A. Sivak, Optimal control in stochastic thermodynamics. *J. Phys. Commun.* **7**, 033001 (2023).
13. M. C. Engel, J. A. Smith, M. P. Brenner, Optimal control of nonequilibrium systems through automatic differentiation. *Phys. Rev. X* **13**, 041032 (2023).
14. S. Whitelam, Demon in the machine: Learning to extract work and absorb entropy from fluctuating nanosystems. *Phys. Rev. X* **13**, 021005 (2023).
15. A. Zhong, M. R. DeWeese, Beyond linear response: Equivalence between thermodynamic geometry and optimal transport. *Phys. Rev. Lett.* **133**, 057102 (2024).
16. A. Zhong, M. R. DeWeese, Limited-control optimal protocols arbitrarily far from equilibrium. *Phys. Rev. E* **106**, 044135 (2022).
17. M. Chatterjee, V. Holubec, R. Marathe, Optimal constrained control for generally damped Brownian heat engines. *J. Phys. A: Math. Theor.* **58**, 245001 (2025).
18. R. Garcia-Millan, J. Schüttler, M. E. Cates, S. A. M. Loos, Optimal closed-loop control of active particles and a minimal information engine. *Phys. Rev. Lett.* **135**, 088301 (2025).
19. J. Schüttler, R. Garcia-Millan, M. E. Cates, S. A. M. Loos, Active particles in moving traps: Minimum work protocols and information efficiency of work extraction. *Phys. Rev. E* **112**, 024119 (2025).
20. D. Abreu, U. Seifert, Extracting work from a single heat bath through feedback. *Europhys. Lett.* **94**, 10001 (2011).
21. E. Aurell, C. Mejía-Monasterio, P. Muratore-Ginanneschi, Optimal protocols and optimal transport in stochastic thermodynamics. *Phys. Rev. Lett.* **106**, 250601 (2011).
22. S. A. M. Loos, S. Monter, F. Ginot, C. Bechinger, Universal symmetry of optimal control at the microscale. *Phys. Rev. X* **14**, 021032 (2024).
23. P. Nazé, Analytical solution for optimal protocols of weak drivings. *J. Stat. Mech: Theory Exp.* **2024**, 073205 (2024).
24. C. Battle *et al.*, Broken detailed balance at mesoscopic scales in active biological systems. *Science* **352**, 604–607 (2016).
25. B. S. Pollard, Open Markov processes: A compositional perspective on non-equilibrium steady states in biology. *Entropy* **18**, 140 (2016).
26. J. F. Rupprecht, J. Prost, A fresh eye on nonequilibrium systems. *Science* **352**, 514–515 (2016).
27. Y. Oono, M. Paniconi, Steady state thermodynamics. *Prog. Theor. Phys. Suppl.* **130**, 29–44 (1998).
28. T. Hatano, Si. Sasa, Steady-state thermodynamics of Langevin systems. *Phys. Rev. Lett.* **86**, 3463 (2001).
29. E. Trepagnier *et al.*, Experimental test of Hatano and Sasa's nonequilibrium steady-state equality. *Proc. Natl. Acad. Sci. U.S.A.* **101**, 15038–15041 (2004).
30. P. R. Zulkowski, D. A. Sivak, M. R. DeWeese, Optimal control of transitions between nonequilibrium steady states. *PLoS ONE* **8**, e82754 (2013).
31. L. K. Davis, K. Proesmans, É. Fodor, Active matter under control: Insights from response theory. *Phys. Rev. X* **14**, 011012 (2024).
32. A. Baldassarri, A. Puglisi, L. Sesta, Engineered swift equilibration of a Brownian gyrator. *Phys. Rev. E* **102**, 030105 (2020).
33. H. Rehage, H. Hoffmann, Rheological properties of viscoelastic surfactant systems. *J. Phys. Chem.* **92**, 4712–4719 (1988).
34. M. Cates, S. Candau, Statics and dynamics of worm-like surfactant micelles. *J. Phys. Condensed Matter* **2**, 6869 (1990).
35. J. Caspers *et al.*, How are mobility and friction related in viscoelastic fluids? *J. Chem. Phys.* **158**, 024901 (2023).
36. C. Jarzynski, Nonequilibrium equality for free energy differences. *Phys. Rev. Lett.* **78**, 2690 (1997).
37. G. E. Crooks, Nonequilibrium measurements of free energy differences for microscopically reversible Markovian systems. *J. Stat. Phys.* **90**, 1481–1487 (1998).
38. F. Ginot *et al.*, Recoil experiments determine the eigenmodes of viscoelastic fluids. *New J. Phys.* **24**, 123013 (2022).
39. T. G. Mason, D. A. Weitz, Optical measurements of frequency-dependent linear viscoelastic moduli of complex fluids. *Phys. Rev. Lett.* **74**, 1250–1253 (1995).
40. S. Yamada, D. Wirtz, S. C. Kuo, Mechanics of living cells measured by laser tracking microrheology. *Biophys. J.* **78**, 1736–1747 (2000), Particle tracking in cell–VE MSD.
41. Y. Mao, P. Nielsen, J. Ali, Passive and active microrheology for biomedical systems. *Front. Bioeng. Biotechnol.* **10**, 916354 (2022), Review with tables of experiments in different bio systems.
42. J. Bradbury *et al.*, JAX: Composable transformations of Python+NumPy programs (2018). GitHub. http://github.com/jax-ml/jax.
43. I. A. Martínez, A. Petrosyan, D. Guéry-Odelin, E. Trizac, S. Ciliberto, Engineered swift equilibration of a Brownian particle. *Nat. Phys.* **12**, 843–846 (2016), CB.
44. D. Blair, E. Dufrense, The MatLab particle tracking code repository (2005). https://site.physics.georgetown.edu/matlab/index.html. Accessed 26 August 2025.
45. DeepMind *et al.*, The DeepMind JAX Ecosystem (2020). GitHub. http://github.com/google-deepmind.
46. S. Monter, S. A. M. Loos, C. Bechinger, Suplementary code. Zenodo. https://doi.org/10.5281/zenodo.16408136. Accessed 24 July 2025.
47. S. Monter, Optimal transitions between non-equilibrium steady states. GitHub. https://github.com/SaMoPhys/opt_con_ness. Accessed 24 July 2025.
48. S. Monter, S. A. M. Loos, C. Bechinger, Data for Optimal transitions between non-equilibrium steady states. Zenodo. https://zenodo.org/records/16979959. Deposited 28 August 2025.